JOURNAL OF MATERIALS SCIENCE: MATERIALS IN MEDICINE **17** (2006) 1–6

The influence of grain size on the ductility of micro-scale stainless steel stent struts

B. P. MURPHY[1,*], H. CUDDY[1,2], F. J. HAREWOOD[1,2], T. CONNOLLEY[1], P. E. MCHUGH[1,2]
[1]*National Centre for Biomedical Engineering Science, National University of Ireland, Galway, Ireland*
E-mail: bruce.murphy@nuigalway.ie
[2]*Department of Mechanical and Biomedical Engineering, National University of Ireland, Galway, Ireland*

Vascular stents are used to restore blood flow in stenotic arteries, and at present the implantation of a stent is the preferred revascularisation method for treating coronary artery disease, as the introduction of drug eluting stents (DESs) has lead to a significant improvement in the clinical outcome of coronary stenting. However the mechanical limits of stents are being tested when they are deployed in severe cases. In this study we aimed to show (by a combination of experimental tests and crystal plasticity finite element models) that the ductility of stainless steel stent struts can be increased by optimising the grain structure within micro-scale stainless steel stent struts. The results of the study show that within the specimen size range 55 to 190 μm ductility was not dependent on the size of the stent strut when the grain size maximised. For values of the ratio of cross sectional area to characteristic grain length less than 1000, ductility was at a minimum irrespective of specimen size. However, when the ratio of cross sectional area to characteristic grain length becomes greater than 1000 an improvement in ductility occurs, reaching a plateau when the ratio approaches a value characteristic of bulk material properties. In conclusion the ductility of micro-scale stainless steel stent struts is sensitive to microstructure and can be improved by reducing the grain size.

Introduction

Vascular stents are used to restore blood flow in stenotic arteries and presently implantation of a stent is the preferred revascularisation method for treating coronary artery disease [1]. Recently the introduction of drug eluting stents (DESs) has lead to a significant improvement in the clinical outcome of coronary stenting; whereby controlled clinical trials show that, after nine months follow-up, the rate of in-stent restenosis can be reduced from 24.4% with bare metal stents, to 5.5% by using an equivalent DES [2]. This reduction of in-stent restenosis has led to confident use of cardiovascular stenting; for example coronary stenting is now selected for patients that would have traditionally been treated by coronary artery bypass surgery [3]. This strategy is exposing the mechanical limits of coronary stents, and fracture of DESs has been reported in two separate cases [4]. Even with reported *in vivo* fractures of stents there is a desire to make stent struts thinner to reduce the crossing profile, increase stent flexibility and decrease the pressure needed for deployment [5]. Furthermore, there are a number of other mechanical and clinical issues concerned with reducing the thickness of stent struts; firstly, the stress-strain behaviour of a stent strut is dependent on size [6]; secondly, the rate of restenosis can be reduced considerably by the use of thinner-strut stents [7–9], and finally, thinner struts are associated with faster re-endothelialisation in comparison to thicker struts [10]. With the beneficial clinical objectives of making stent struts thinner [7–10] and the use of stenting in complex situations [4] there is a need to optimise the material properties of smaller stent struts to maintain safety standards and to design stents to maximise their *in vivo* performance.

*Author to whom all correspondence should be addressed.

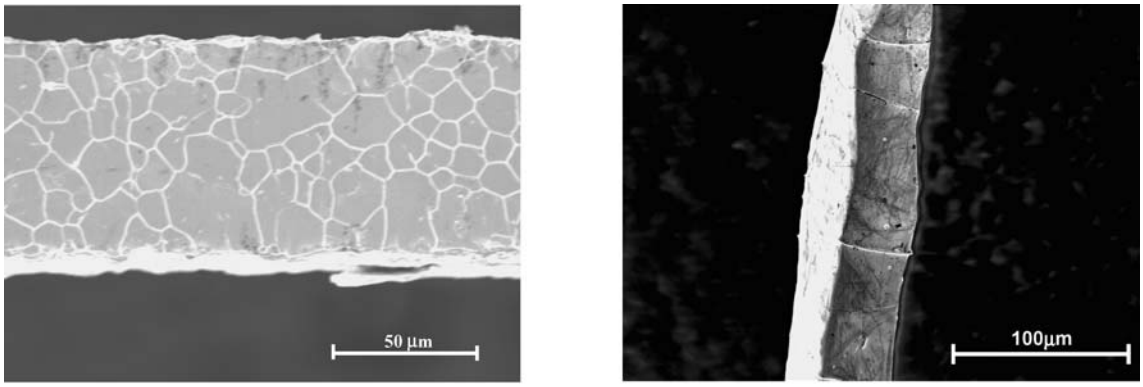

(a) (b)

Figure 1 (a) shows an etched specimen with an average grain area of 92 μm^2–similar to the specimens tested in [6]. The white lines on the specimen correspond to grain boundaries. (b) shows a highly annealed specimen that has been tensile tested and etched post testing, faint lines on the specimen indicate grain boundaries; this example shows that only one grain exists through the thickness of the stent strut.

Stainless steel (Grade 316LVM) is the most common material used in coronary stents [11], and when these stents are crimped onto balloon catheters or dilated during angioplasty plastic deformation occurs. At present bulk properties are used to describe the stress-strain behaviour of the material at the small size scale of coronary stents, although it may be argued that the relative size of the grains, 25 μm [12] versus strut thickness (70–120 μm) [11] may affect the material properties at this size scale. Previous work has shown that the stress-strain behaviour of 316L stainless steel stent struts is size dependent [6], and similarly the ductility of relatively large modified 316 austenitic stainless steel specimens showed significant dependence on specimen aspect ratio [13]. In Savage *et al.* [14] the mechanism for the 316L stent strut size effect reported in [6] was explored using micromechanical finite element modelling; the mechanism was shown to be related to constraint of plastic deformation at the grain level in the material. Furthermore Meyer-Kobbe and Hinrichs [15] alluded to the fact that the material properties of 316LVM stents can be altered by changing the annealing conditions. The above evidence suggests that optimisation of the material properties of small scale stainless steel stent struts is possible, and moreover is essential if the thickness of stent struts is reduced to accommodate clinical concerns [5, 7–10].

This study hypothesises that there is a range of ductility values for constant thickness stent struts, and that the ductility can be optimised depending on the average grain size in the stent strut. To test this hypothesis a series of experimental tests were performed in parallel with predictive crystal plasticity finite element simulations that were based on the models presented in Savage *et al.* [14].

Materials and methods

Experimental tensile testing was performed on highly annealed 316L stainless steel stent struts. The specimens were manufactured to produce stent struts with a minimum number of grains through the width or thickness, and in most cases only one grain existed through the width or thickness. This type of grain structure was accomplished by a separate annealing step, whereby the specimens were annealed for two hours at 1100 °C. This process produced stent struts with an average grain area of 6973 μm^2, in comparison to an average grain area of 92 μm^2 for the specimens considered by Murphy *et al.* [6]. Examples of the grain structure of highly annealed stent struts can be observed in Fig. 1.

The specimens were prepared by laser cutting their profile from 1.75 mm diameter tubes and subsequently being electro-polished to a constant wall thickness of 85 μm. Three different widths were investigated 55, 110 and 190 μm, six specimens were tested for the 55 and 110 μm groups while only two specimens were available for testing at the 190 μm size. All specimens had a gauge length of 4 mm (see Fig. 2 in [6] for a schematic of the laser cut specimens used). The tensile testing methodology and the gripping system used was previously described in detail in Murphy *et al.* [6].

Finite element models

The simulations performed in this work were based on large strain (finite deformation) kinematics and incorporated an elastic-plastic constitutive description of the material. The ABAQUS® finite element code was used for the simulations. Elasticity was considered as being linear in terms of finite deformation quantities, and plasticity was described using crystal plasticity theory, which attempts to represent the flow of dislocations along slip systems in metallic crystals in terms of continuum plastic shear strains. In particular, the rate-dependent single crystal formulation of the theory, presented in Pierce *et al.* [16], Huang [17], and McGarry *et al.* [18], was used.

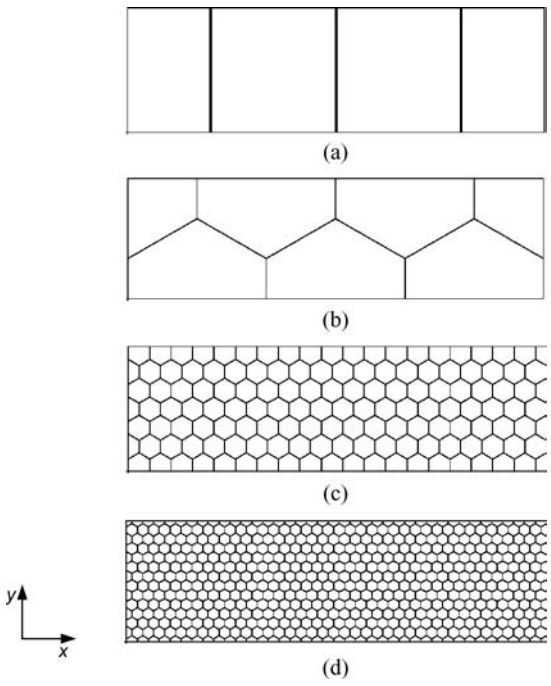

Figure 2 Schematic of the grain representations for the four different models used, (a) shows the one grain model which is similar to the fractograph presented in Fig. 1(b). The remaining three models use hexagons to describe the grain structure where (b) is the two grain model, (c) has seven grains through the thickness, while (d) has 14 grains through the thickness.

In crystal plasticity theory, plastic slip is assumed to obey Schmidt's law, where the rate of plastic shear strain in the direction of a particular slip system α, $\dot{\gamma}^{(\alpha)}$, is assumed to depend on the Schmidt resolved shear stress for that slip system (on the slip plane, in the direction of the slip system), $\tau^{(\alpha)}$. In this work, the following power-law rate-dependent relationship was used:

$$\dot{\gamma}^{(\alpha)} = \dot{a}\mathrm{sgn}\left(\tau^{(\alpha)}\right)\left\{\left|\frac{\tau^{(\alpha)}}{g^{(\alpha)}}\right|\right\}^{n} \tag{1}$$

where $\dot{a}$ and n are the reference strain rate and rate sensitivity exponent, respectively. Material strain hardening is specified by the slip system strain hardness, $g^{(\alpha)}$. This, in turn, as detailed in [16–18], is related to the strain hardness function, g, for the crystal. The following form of the strain hardness function (Pierce *et al.* [16]) was used:

$$g(\gamma_a) = g_0 + (g_\infty - g_0)h_0\tanh\left|\frac{h_0\gamma_a}{g_\infty - g_0}\right| \tag{2}$$

This function involves three material strain hardening constants, g_0, g_∞ and h_0, that must be determined by fitting to experimental tensile stress-strain data. g is a function of the *accumulated slip*, γ_a, which is a measure of the total crystallographic plastic strain at a material point in the crystal and is defined as follows:

$$\gamma_a = \sum_\alpha \int_0^t \left|\dot{\gamma}^{(\alpha)}\right| dt \tag{3}$$

where t is time and the summation ranges over all slip systems at the point. The theory was implemented numerically in ABAQUS® via a UMAT–user material subroutine due to Huang [17].

TABLE I Finite element model parameters

	No. of grains	Average grain area (mm^2)	Number of elements	Average elements/grain
Model 1	4	3.0×10^{-3}	588	147
Model 2	7	1.78×10^{-3}	600	85
Model 3	119	8.54×10^{-5}	13,377	112
Model 4	546	2.16×10^{-5}	51,205	94

Four different finite element models were generated representing four different idealised grain configurations: a one grain width model, two grain model, seven grain model, and a model with 14 grains through the width, Fig. 2 shows a schematic of the four models. The geometry of the models was kept constant, a thickness of 80 μm, width of 60 μm and a length of approximately 200 μm was used. The number of grains, elements, average number of elements per grain and average grain size is presented in Table I. The boundary conditions, for all the models involved, restraining the left hand side of the model in the x and y direction, and applying a displacement in the x direction to the right hand side of the model at a rate of 1mm/min, which is identical to the displacement rate in the experiments. The models were 2D models consisting of 8-noded generalised plane strain quadrilateral elements. The material properties used were as follows: Young's modulus, $E = 193$ GPa and Poisson's Ratio, $\nu = 0.3$. The strain hardening values used in this study were: $g_0 = 150$ MPa, $g_\infty = 360$ MPa and $h_0 = 380$ MPa. The parameters $\dot{a} = 0.0106\ \mathrm{s}^{-1}$ and $n = 50$ were also used. These values were determined from experimental data for 316L stainless steel [19]. A random 3D FCC lattice orientation was assigned to each of the grains causing lattice mismatch at the grain boundaries; this process was repeated five times for each model, producing a dataset of 20 models, with $N = 5$ for each grain configuration. As established in [14] these generalised plane strain models with 3D crystal lattice configurations can be reliably used to elucidate the relationship between the polycrystalline microstructure of the material and its macroscopic mechanical behaviour.

Results

The results show that ductility is at a minimum for single grain specimens (in the size range 55 to 190 μm)

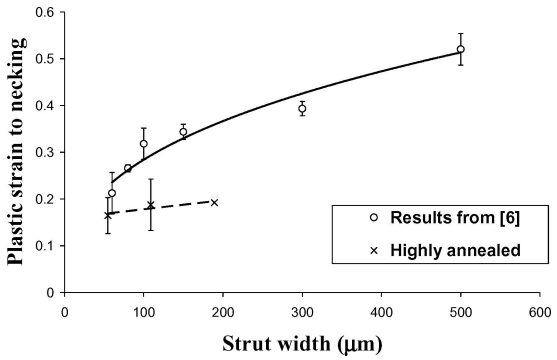

Figure 3 Plot of the plastic strain to necking versus strut width for highly annealed specimens and the data from [6] has been replotted for comparison purposes; average values are shown and error bars indicating one standard deviation either side of the average are shown.

when compared to the results presented in [6]. Fig. 3 shows a plot of the strain to necking versus strut width for the highly annealed specimens, and for comparison purposes the results of [6] have been replotted. The slope of the regression line fitted to the highly annealed data is approximately zero ($m = 0.0002$) while a linear trendline fitted (not shown) to the results of [6] has a slope 3 times greater ($m_{[6]} = 0.0006$), emphasising the point that there is no difference in strain at necking between any of the highly annealed specimen groups. Furthermore, a Student's T-test reveals no statistically significant difference in plastic strain to necking between the three sizes.

A comparison of the computational results is shown in Fig. 4; these results show that the strain to necking is dependent on the number of grains through the thickness of the strut, and the trend revealed shows that the strain to necking reduces as the number of grains through the thickness decreases. The results reveal that there is no statistically significant difference between the one and two grain models and the two and seven grain models, while there is a statistically significant difference between every other group (Student's T-test $p < 0.05$). A comparison of the experimental and computational results for the 60 μm specimens shows that the above trend is confirmed in both the experimental and computational results (see Fig. 5) whereby ductility reduces as average grain area increases.

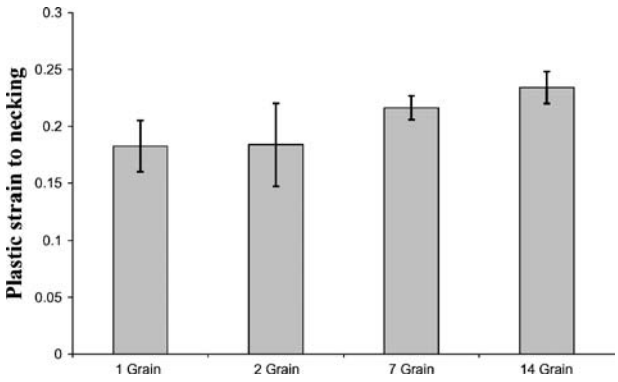

Figure 4 Plot of the plastic strain to necking for the four different finite element models.

Discussion

The results of the experimental study show that a ductility size effect is primarily associated with grain size. This conclusion is drawn, as all the highly annealed specimens have a consistent grain structure through their thickness, i.e. one to two grains for all three specimen sizes tested, and secondly the results demonstrate no statistically significant difference in strain to necking in the size range 55–190 μm. This is in comparison to the results presented in [6], which exhibit the largest difference in ductility size dependence at this size range. However there is a slight size effect associated with the highly annealed specimens, this can be seen by the small positive slope ($m = 0.0002$) associated with a trendline plotted through the highly annealed data set. This effect may be associated with defects in the samples, i.e. a smaller sample would have a lower strain to failure if a defect was present in comparison to a larger specimen. One experimental observation was that the highly annealed specimens exhibited multiple necking regions in comparison to the results of [6] which only exhibited a single necking region. The multiple necking regions would reduce the strut failure strain as the probability of early failure increases in the highly annealed specimens due to multiple areas of non-uniform strain caused by weak single grains passing through the width/thickness of the specimen. Furthermore, the difference in the results of [6] versus the highly annealed specimens of this study shows that a range of ductility values can be achieved for a constant thickness specimen if the grain size is altered. This range would have a lower boundary associated with the ductility of the highly annealed specimens (i.e. one/two grains through the thickness) while the upper boundary of the range would be defined by the bulk specimen properties.

The computational and experimental studies predict that the ductility range for constant width specimens of various grain sizes is non-linear; this fact is illustrated in Fig. 5, where the x-axis is plotted on a logarithmic scale. The lower boundary of this range was reached with either the one or the two-grain models, as the results show no improvement in ductility between these two models. The difference between the seven and fourteen-grain models is more pronounced, with ductility increasing significantly in the fourteen-grain model in comparison to the seven-grain model. As the relationship between ductility and grain area is non-linear, the ductility could be dramatically increased further if grain size could be reduced further. For example the ductility of bulk specimens could be approached, i.e. 50%

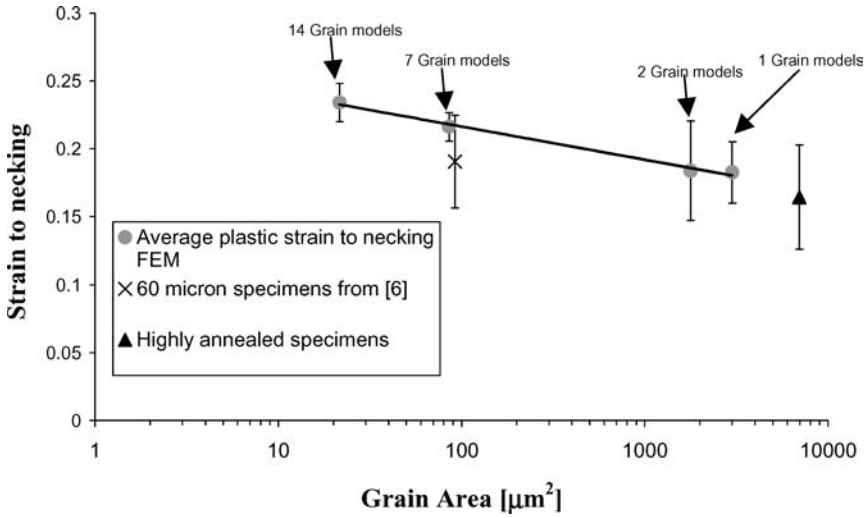

Figure 5 Plastic strain to necking versus grain area is plotted for the experimental tests (both highly annealed (55 μm width) and specimens 60 μm width from [6]), and the results for the computational study are plotted for the four different models all with a constant width of 60 μm. The x-axis is plotted on a logarithmic scale showing that the relationship between grain area and plastic strain to necking is non-linear.

plastic strain to failure, which is similar to the strain to necking of the 500 μm specimens tested in [6]. This group of specimens has a characteristic grain length[1] to strut width ratio of 84 (assuming a hexagonal grain shape), while the fourteen-grain finite element models have a characteristic grain length to strut width ratio of 20.8 demonstrating that further increases in ductility for 60 μm specimens can be attained if the grain size was made smaller than the size of the grains in the fourteen-grain model. This ratio is directly proportional to the cross sectional area (CSA) to characteristic grain length ratio which depends on both the strut width and thickness, but importantly takes account of the minimum dimension. A plot of the ratio of the CSA to characteristic grain length versus strain to necking (for all the experimental specimens, including data from [6], and the finite element models) shows that no improvement in strain to necking is achieved within a range of CSA to characteristic grain size ratio of 10 to approximately 1000, while an improvement in ductility is attained by increasing this ratio further than 1000, see Fig. 6.

Furthermore, it is important to note the very good quantitative agreement between experimentally measured necking strains and those predicted by the finite element models (Fig. 5). This represents an improvement in the quantitative prediction capabilities of the models, in comparison to the results presented in [14]; this is chiefly due to the use of the material parameters determined in [19]. The agreement also justifies the applicability of the 2D generalised plane strain modelling approach.

[1]The characteristic grain length is defined as the side length of a hexagon that would represent the equivalent area of an irregular grain.

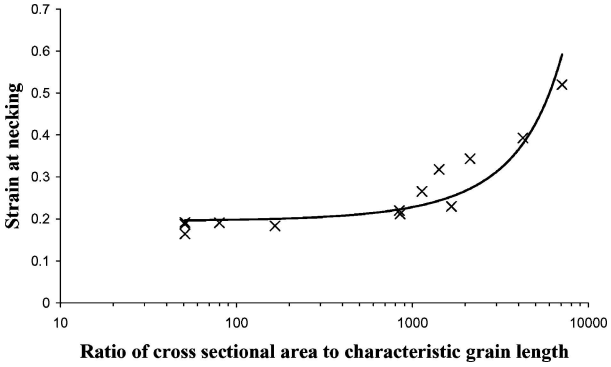

Figure 6 Plot of the ratio of the CSA to characteristic grain length for all the experimental and computational results. The characteristic grain length refers to the side length of an idealised grain i.e. hexagonal in shape; it was assumed that all the grains could be represented as hexagons, excluding the one-grain FE models where the grains were modelled as rectangles. The data points represent the averages for the finite element models and the averages for the experimental data.

Conclusions

The results of this study suggest that making the grains as small as possible in comparison to the strut CSA would increase the ductility of stainless steel stents and allow them to be used with greater confidence in more adverse conditions. In addition, a number of specific conclusions can be drawn from this work, namely:

1. A ductility size effect in micro-scale stainless steel components is primarily associated with grain size.
2. No improvement in ductility is achieved within a range of CSA to characteristic grain size ratios of 10 to approximately 1000, while an improvement in

ductility is attained by increasing this ratio further than 1000.

3. Excellent quantitative agreement was achieved between the experimentally measured necking strains and those predicted by the crystal plasticity finite element models by using updated material properties.

Acknowledgements

The authors with to acknowledge funding from the Programme for Research in Third Level Institutions (PRTLI), administered by the Higher Education Authority, the Irish Research Council for Science, Engineering and Technology, and from Enterprise Ireland. The authors wish to thank Dr. David Quinn of Medtronic Ltd. for the provision of stent strut specimens and Dr. Mark Bruzzi for the fractograph of an etched specimen. The simulations in this work were performed on the SGI 3800 high performance computer at NUI, Galway.

References

1. E. J. TOPOL, *New Engl. J. Med.* **339** (1998) 1702.
2. A. HALKIN and G. W. STONE, *J. of Interventional Cardiology* **17** (2004) 271.
3. R. T. VAN DOMBURG, P. A. LEMOS, J. M. TAKKENBERG, T. K. K. LIU and L. A. VAN HERWERDEN, *et al.*, *Eur. Heart J.* 2005 (in press).
4. G. SIANOS, S. HOFMA, J. M. R. LIGTHART, F. SAIA, A. HOYE, P. A. LEMOS and P. W. SERRUYS, *Catherization and Cardiovascular Interventions* **61** (2004) 111.
5. D. R. HOLMES and D. J. KEREIAKES, *Reviews in Cardiovascular Medicine* **6**(Suppl. 1) (2005) 31.
6. B. P. MURPHY, P. SAVAGE, P. E. MCHUGH and D. F. QUINN, *Ann. Biomed. Eng.* **31** (2003) 686.
7. J. PACHE, A. KASTRATI, J. MEHILLI, H. SCV̈HLEN, F. DOTZER and J. HAUSLEITER, *et al.*, *Journal of the American College of Cardiology* **41** (2003) 1283.
8. A. KASTRATI, J. MEHILLI, J. DIRSCHINGER, F. DOTZER and H. SCV̈HLEN, *et al. Circulation* **103** (2001) 2816.
9. S. Z. H. RITTERSMA, R. J. DE WINTER, K. T. KOCH, M. BAX and C. E. SCHOTBORGH, *et al. American Journal of Cardiology* **93** (2004) 477.
10. C. SIMON, J. C. PALMAZ and E. A. SPRAGUE, *Journal of Long-Term Effects of Medical Implants* **10**(1/2) (2000) 143.
11. P. W. SERRUYS and M. J. B. KUTRYK, in "Handbook of Coronary Stents" (Martin Dunitz Ltd., London 2000)
12. D. MÖLLER, W. REIMERS, A. PYZALLA and A. FISCHER, *J. Biomed. Mater. Res.* **58** (2001) 69.
13. Y. KOHNO, A. KOHYAMA, M. L. HAMILTON, T. HIROSE, Y. KATOH and F. A. GARNER, *J. Nucl. Mater.* **283–287** (2000) 1014.
14. P. SAVAGE, B. P. O'DONNELL, P. E. MCHUGH, B. P. MURPHY and D. F. QUINN, *Ann. Biomed. Eng.* **32** (2004) 202.
15. C. MEYER-KOBBE and B. H. HINRICHS, *Medical Device Technology* **14**(1) (2003) 20.
16. D. PIERCE, R. J. ASARO and A. NEEDLEMAN, *Acta Metall. Mater.* **31** (1983) 1951.
17. Y. HUANG, A User-Material Subroutine Incorporating Single Crystal Plasticity in the ABAQUS Finite Element Program. Harvard University Report, MECH 178 1991.
18. J. P. MCGARRY, B. P. O'DONNELL, P. E. MCHUGH and J. G. MCGARRY, *Comput. Mater. Sci.* **31** (2004) 421.
19. X. YOU, T. CONNOLLEY and P. E. MCHUGH, Manuscript in Preparation, 2005.

Received 6 May 2005
and accepted 24 May 2005